

Identification of three cataclysmic variables detected by the ART-XC and eROSITA telescopes on board the SRG during the all-sky X-ray survey

Zaznobin I.^{1,2}, Sazonov S.^{1,3}, Burenin R.^{1,2}, Uskov G.¹, Semena A.¹, Gilfanov M.^{1,3}, Medvedev P.¹, Sunyaev R.^{1,3}, and Eselevich M.⁴

¹ Space Research Institute, 84/32 Profsovnaya str., Moscow 117997, Russia

² Sternberg Astronomical Institute, 14 Universitetskij pr., Moscow, Russia

³ Moscow Institute of Physics and Technology, Institutsky per. 9, 141700 Dolgoprudny, Russia

⁴ Max-Planck-Institut für Astrophysik (MPA), Karl-Schwarzschild-Str. 1, D-85741 Garching, Germany

⁵ Institute of Solar-Terrestrial Physics, Russian Academy of Sciences, Siberian Branch, Irkutsk, Russia

December 10, 2021

ABSTRACT

We report the discovery of three cataclysmic variables in the data of the first year of the all-sky X-ray survey by the *SRG* orbital observatory. The sources were selected for their brightness in the 4–12 keV band in the data of the Mikhail Pavlinsky ART-XC telescope. They are also detected by the eROSITA telescope, which provides accurate localizations and spectral data for a broadband spectral analysis. All three objects were previously known as X-ray sources from the *ROSAT* all-sky survey and *XMM-Newton* slew survey, but their nature remained unknown. The X-ray spectra obtained by eROSITA and ART-XC are consistent with optically thin thermal emission with a temperature $kT \gtrsim 18$ keV for SRGA J194638.9+704552 and SRGA J225412.8+690658 and $kT \gtrsim 5$ keV for SRGA J204547.8+672642. Together with the inferred high X-ray luminosities ($2 \times 10^{32} - 3 \times 10^{33}$ erg s⁻¹), this strongly suggests that all three sources are cataclysmic variables (CVs). We have obtained optical photometry and spectroscopy for these objects using the AZT-33IK 1.6 m telescope of the Sayan Observatory. The optical properties confirm the CV nature of the objects. We conclude that SRGA J194638.9+704552 is an intermediate polar, SRGA J204547.8+672642 is likely a polar or intermediate polar, and SRGA J225412.8+690658 is either a magnetic or nonmagnetic CV. We have also measured an orbital period of 2.98 hours for SRGA J204547.8+672642 based on *TESS* data. Three out of the planned eight *SRG* all-sky surveys have now been completed. We expect to find many new CVs, in particular, magnetic systems, during the survey, and we plan to continue our optical follow-up program.

Key words. (Stars:) novae, cataclysmic variables - Surveys - Catalogs - X-rays: stars

1. Introduction

The *Spectrum-Roentgen-Gamma* (*Spektr-RG*, *SRG*) orbital observatory (Sunyaev et al. 2021) has been carrying out an all-sky X-ray survey since 12 December 2019. The survey is planned to consist of eight consecutive scans of the entire sky, each lasting six months. The *SRG* payload consists of two grazing-incidence telescopes: the extended ROentgen Survey with an Imaging Telescope Array (eROSITA, Predehl et al. 2021), and the Mikhail Pavlinsky Astronomical Roentgen Telescope – X-ray Concentrator (ART-XC, Pavlinsky et al. 2021b). They operate in the overlapping 0.2–8 keV and 4–30 keV energy bands, respectively. The *SRG* survey is unique in a number of ways. In the soft X-ray band (0.2–2.3 keV), eROSITA is expected to detect several million X-ray sources, which is a factor of $\gtrsim 30$ more than during the Röntgensatellit (*ROSAT*) all-sky survey (Boller et al. 2016) that was conducted 30 years ago. At higher energies, eROSITA and ART-XC will survey the whole sky with subarcminute angular resolution for the first time. The ART-XC survey in the 4–12 keV energy band is expected to significantly surpass the previous surveys that were carried out in similar

(medium X-ray) energy bands in terms of the combination of angular resolution, sensitivity, and uniformity. The *SRG* all-sky survey is expected to have a huge impact on our knowledge of various populations of Galactic and extragalactic objects. Initial results of the mission demonstrate that it meets these expectations (Sunyaev et al. 2021).

Recently, a catalog of sources detected in the 4–12 keV band by ART-XC during the first year of the all-sky survey (namely, on a combined map of the first and second scans of the sky; ART-XC Sky Surveys 1 and 2, or ARTSS12) has been produced (Pavlinsky et al. 2021a) that comprises 867 sources. Most of them (~ 750) are previously known astrophysical objects, the largest group of which are active galactic nuclei (AGN; ~ 370), followed by X-ray binaries (~ 170) and cataclysmic variables (CVs; ~ 100 , including symbiotic systems)¹.

To place the number of CVs that have been detected by ART-XC into context, we note that the published samples of CVs selected in soft X-rays (0.1–2.4 keV) from the *ROSAT* all-sky survey comprise ~ 50 objects (Schwope et al. 2002; Pretorius & Knigge 2012; Pretorius et al. 2013), while the sample of CVs from the *RXTE* slew survey in the 3–20 keV band in-

Send offprint requests to: Zaznobin I., e-mail: zaznobin@iki.rssi.ru

¹ The approximate sign before the quoted numbers indicates that for some of the objects the suggested classification is currently not reliable.

cludes ~ 25 objects (Sazonov et al. 2006). Recently, samples of ~ 100 CVs have been obtained thanks to serendipitous hard X-ray (above 15 keV) surveys carried out by the *INTErnational Gamma-Ray Astrophysics Laboratory* (*INTEGRAL*) and *Swift* observatories (Revnitsev et al. 2008; Oh et al. 2018; Lutovinov et al. 2020). These data have been accumulated over ~ 15 years. It is expected that ART-XC will increase the sample of X-ray selected CVs by several times over the course of the four-year survey to up to ~ 500 objects. This sample will be of high value for systematic population studies of CVs because the 4–12 keV energy band is ideally suited for selecting CVs of virtually all classes (both magnetic and nonmagnetic, see Mukai 2017 for a recent review): It is hardly affected at all by the low-energy (due to photoabsorption) and high-energy cutoffs that are observed in the broadband X-ray spectra of CVs.

We have started a program of optical follow-up observations of the new and previously unidentified X-ray sources in the ARTSS12 catalog. This has already led to the identification of several AGN, including heavily obscured ones (Zaznobin et al. 2021). In this paper, we present the results of the identification of three more ART-XC sources that have been proved to be CVs.

2. Sample

The objects for this study (see Table 1) were selected from the catalog of point sources detected by the ART-XC telescope on the combined map of the first and second sky surveys (12 December 2019 – 15 December 2020) with a signal-to-noise ratio (S/N) higher than 4.8 in the 4–12 keV energy band. The positions of the sources were measured with an accuracy of better than $30''$ (at 95% confidence). All three sources have also been detected by eROSITA, which allowed us to improve their positions to within a few arcseconds (see Table 1) and to construct their X-ray spectra in a broad energy range from 0.2 to 20 keV (using both eROSITA and ART-XC data).

All three objects were discovered as X-ray sources during the *ROSAT* all-sky survey (RASS) and were later also detected during the *XMM-Newton* slew survey (Saxton et al. 2008), but have remained unidentified until now. The improved localizations provided by the *SRG* and the advent of recent optical all-sky surveys (in particular, *Gaia*), have made it straightforward to identify an optical counterpart for each of these X-ray sources. Table 1 provides for each object the ART-XC and eROSITA positions, the coordinates of the optical counterpart according to the *Gaia* early data release (EDR3) catalog (Gaia Collaboration et al. 2021), and the name of the source in the second *ROSAT* all-sky survey (2RXS) source catalogue (Boller et al. 2016).

3. X-ray observations

All three objects have by now been observed during the first three *SRG* all-sky surveys. As a result of their high ecliptic latitudes ($b_{\text{ecl}} = 79.5^\circ, 74.1^\circ, \text{ and } 63.8^\circ$ for SRGA J194638.9+704552, SRGA J204547.8+672642, and SRGA J225412.8+690658, respectively) and the strategy of the *SRG* survey (namely, scanning great circles that intersect at the ecliptic poles; see Sunyaev et al. 2021), all three sources received relatively long observing times. Specifically, the *SRG* visited them over periods of 3–5 days during each all-sky survey, compared to ~ 1 day for typical sources at low ecliptic latitudes. However, in reality, each of these visits consisted of a few dozen short (~ 20 s and ~ 40 s for ART-XC and eROSITA, respectively) passages separated by 4 hours, so that the total accumu-

lated exposure times are just ~ 1 ks for ART-XC and a factor of ~ 4 longer for eROSITA² (see Table 2).

In what follows, we focus on the fluxes and spectra of the sources averaged over all available *SRG* observations. Table 2 provides the average fluxes in the 0.3–2.2 and 4–12 keV energy bands, where the maximum sensitivity is achieved by eROSITA and ART-XC, respectively (Sunyaev et al. 2021).

We also provide in Table 2 the column densities of neutral hydrogen throughout the Galaxy, $N_{\text{H,Gal}}$, in the direction of the objects (HI4PI Collaboration et al. 2016). Because the distances to the sources are all larger than ~ 700 pc and they are located relatively high above the Galactic plane ($b = 21.1^\circ, 14.9^\circ, \text{ and } 8.6^\circ$ for SRGA J194638.9+704552, SRGA J204547.8+672642, and SRGA J225412.8+690658, respectively), we may expect the bulk of the Galactic HI column to be located between us and the objects. This issue is discussed in more detail in Section 4.

3.1. Spectral analysis

Based on the eROSITA and ART-XC data, we performed an X-ray spectral analysis in the 0.2–12 keV energy range for SRGA J204547.8+672642 and SRGA J225412.8+690658 and in the 0.2–20 keV range for SRGA J194638.9+704552. The eROSITA raw data were processed by the calibration pipeline at the Space Research Institute (IKI, Moscow), which was built using the components of the eROSITA Science Analysis Software System (eSASS).

We extracted the source spectra and light curves using a circular region with a radius of 60 arcsec centered on the source position. An annulus region with the inner and outer radii of 150 and 300 arcsec around each source was used for background extraction. We masked out the circular regions of 40 arcsec radius around all sources that overlap with the studied sources and background regions and detected with $S/N > 4$. The eROSITA spectra were binned to have at least 25 counts in each spectral interval.

We processed the ART-XC data with the analysis software ARTPRODUCTS v0.9 (Pavlinisky et al. 2021b) using the calibration files version 20200401. We tried to extract counts in the 4–7, 7–12, and 12–20 keV energy intervals for all three sources. However, SRGA J204547.8+672642 and SRGA J225412.8+690658 have very few counts in the 12–20 keV bin. Therefore, we only used the 4–7 and 7–12 keV channels in the spectral analysis of these two sources.

We performed the spectral analysis using *XSPEC*³ v12.11.0. (Arnaud 1996) and assessed the quality of spectral fits using a χ^2 statistic. For some of the spectral models discussed below, the parameter uncertainties were estimated using Monte Carlo Markov chains (MCMC) based on the Goodman–Weare algorithm (Goodman & Weare 2010) with 15×10^3 steps (namely for SRGA J225412.8+690658 in the case of *apec*). No cross-normalization constant between the eROSITA and ART-XC data is used below because introducing this coefficient does not lead to a significant improvement in the spectral fit quality.

3.2. Models

We first tried to describe the spectra by a power-law model modified by photoabsorption (*phabs*powerlaw* model in *XSPEC*) and obtained satisfactory fits in all three cases

² The fields of view of ART-XC and eROSITA are 36 arcmin and 1 deg, respectively.

³ <https://heasarc.gsfc.nasa.gov/xanadu/xspec/>

Table 1. Source list.

| ART-XC source | eROSITA position | | | Gaia position | | RASS name |
|-----------------------|------------------|-----------|----------|---------------|-------------|-----------------------|
| | RA | Dec | R_{98} | RA | Dec | |
| SRGA J194638.9+704552 | 19 46 38.2 | +70 45 58 | 4.1'' | 19 46 38.09 | +70 45 55.6 | 2RXS J194639.7+704551 |
| SRGA J204547.8+672642 | 20 45 48.0 | +67 26 43 | 6.8'' | 20 45 48.04 | +67 26 43.1 | 2RXS J204548.4+672629 |
| SRGA J225412.8+690658 | 22 54 13.0 | +69 07 06 | 3.5'' | 22 54 12.99 | +69 07 06.1 | 2RXS J225416.1+690705 |

Notes. R_{98} is the eROSITA source localization radius at 98% confidence.

Table 2. List of X-ray observations.

| Source | Dates | Exp. ^a ks | $F_{4-12\text{keV}}^b$ 10^{-12} erg s ⁻¹ cm ⁻² | $F_{0.3-2.2\text{keV}}^c$ 10^{-12} erg s ⁻¹ cm ⁻² | $N_{\text{H,Gal}}^d$ 10^{22} cm ⁻² |
|-----------------------|--|-------------------------|---|--|--|
| SRGA J194638.9+704552 | 2020 Jan. 22–24, July 22–24, 2021 Jan. 16–19, 21 | 1.7 | 5.7 ± 0.7 | $2.03^{+0.02}_{-0.03}$ | 0.08 |
| SRGA J204547.8+672642 | 2020 Jan. 3–7, July 1–5, 2021 Jan. 2–6 | 1.8 | 2.3 ± 0.5 | $0.77^{+0.02}_{-0.03}$ | 0.14 |
| SRGA J225412.8+690658 | 2020 Jan. 27–30, July 28–31, 2021 Jan. 21–23 | 1.1 | 1.9 ± 0.7 | $0.25^{+0.01}_{-0.01}$ | 0.41 |

Notes. ^(a) Total ART-XC exposure on the source.

^(b) ART-XC flux in the 4–12 keV energy band averaged over the three sky surveys, estimated assuming a Crab-like spectrum.

^(c) eROSITA flux in the 0.3–2.2 keV energy band averaged over the three sky surveys, estimated using the best-fit absorbed power-law spectral models from Table 3.

^(d) Galactic HI column density from HI4PI Collaboration et al. (2016).

The flux errors correspond to the 68% confidence level.

Table 3. X-ray spectral properties.

| Parameter | SRGA source | | |
|-----------------------|------------------------------------|---------------------------------------|------------------------------------|
| | 194638.9+704552 | 204547.8+672642 | 225412.8+690658 |
| <i>POWER LAW</i> | | | |
| N_{H}^a | $0.12^{+0.02}_{-0.02}$ | $0.25^{+0.04}_{-0.06}$ | $0.50^{+0.24}_{-0.13}$ |
| Γ | $1.3^{+0.1}_{-0.1}$ | $1.6^{+0.2}_{-0.2}$ | $0.8^{+0.3}_{-0.3}$ |
| norm | $9.8^{+0.6}_{-0.6} \times 10^{-4}$ | $5.0^{+0.9}_{-0.7} \times 10^{-4}$ | $1.8^{+0.8}_{-0.5} \times 10^{-4}$ |
| χ^2 | 182.9 | 77 | 7.7 |
| dof ^c | 167 | 47 | 10 |
| <i>BREMSSTRAHLUNG</i> | | | |
| N_{H} | $0.11^{+0.01}_{-0.01}$ | $0.19^{+0.03}_{-0.03}$ | $0.69^{+0.17}_{-0.14}$ |
| kT^b | 40^{+53}_{-17} | 10^{+15}_{-4} | > 21 |
| norm | $1.8^{+0.4}_{-0.2} \times 10^{-3}$ | $6.3^{+0.8}_{-0.4} \times 10^{-4}$ | $7.9^{+0.8}_{-3.2} \times 10^{-4}$ |
| χ^2 | 182.9 | 77.0 | 10.7 |
| dof | 167 | 47 | 10 |
| <i>APEC</i> | | | |
| N_{H} | $0.11^{+0.01}_{-0.01}$ | $0.20^{+0.03}_{-0.02}$ | $0.71^{+0.24}_{-0.11}$ |
| kT | > 18 | $7.1^{+3.8}_{-1.7}$ | > 18 |
| norm | $5.1^{+0.9}_{-0.7} \times 10^{-3}$ | $1.65^{+0.13}_{-0.12} \times 10^{-3}$ | $1.7^{+0.2}_{-0.4} \times 10^{-3}$ |
| χ^2 | 184.6 | 72.2 | 11.9 |
| dof | 167 | 47 | 10 |

Notes. ^(a) Hydrogen column, in units of 10^{22} cm⁻²

^(b) Temperature in keV.

^(c) Degrees of freedom.

The errors and limits correspond to the 90% confidence level.

(Table 3). The inferred absorption columns along the line of sight, N_{H} , are marginally higher than the total Galactic columns of neutral hydrogen in the direction of SRGA J194638.9+704552 and SRGA J204547.8+672642, whereas for SRGA J225412.8+690658, N_{H} is consistent with $N_{\text{H,Gal}}$. All three spectra are hard. The inferred photon indices $\Gamma < 1.8$ are suggestive of thermal emission of an optically thin plasma and typical of CVs, both magnetic and nonmagnetic CVs (e.g., Byckling et al. 2010; Burenin et al. 2016b).

To investigate this hypothesis further, we fitted the spectra with an absorbed thermal bremsstrahlung model (*phabs*bremss*). This resulted in nearly the same fit quality (see Table 3). We can place reliable lower limits on the temperature of the plasma of $kT \gtrsim 20$ keV for SRGA J194638.9+704552 and SRGA J225412.8+690658 and $kT \gtrsim 5$ keV for SRGA J204547.8+672642. Figure 1 shows the best fits for this model.

We next tried to describe the spectra by the *apec* model for a collisionally ionized diffuse gas. As expected, this did not lead to a significant improvement in the fit quality compared to *bremss* for SRGA J194638.9+704552 and SRGA J225412.8+690658 because for such high temperatures as inferred here the plasma is expected to be nearly fully ionized, with no strong emission lines produced (except for weak lines of H- and He-like Fe and Ni near 7 keV, which include too few photons in the spectra to make a difference). For these sources, the lower limits on the plasma temperature inferred from the *apec* model, $kT \gtrsim 18$ keV, are somewhat less stringent than the corresponding values for *bremss*. For SRGA J204547.8+672642, *apec* provides a minor improvement in the fit quality over *bremss* and bounds the plasma temperature within a relatively narrow interval around $kT \sim 7$ keV. This indicates the presence of non-negligible line emission in the eROSITA spectrum of this source.

In summary, both the estimated X-ray luminosities ($\sim 10^{32}$ – 10^{33} erg s⁻¹) and the X-ray spectra being consistent with emission from hot, optically thin plasma strongly indicate that all three sources are CVs.

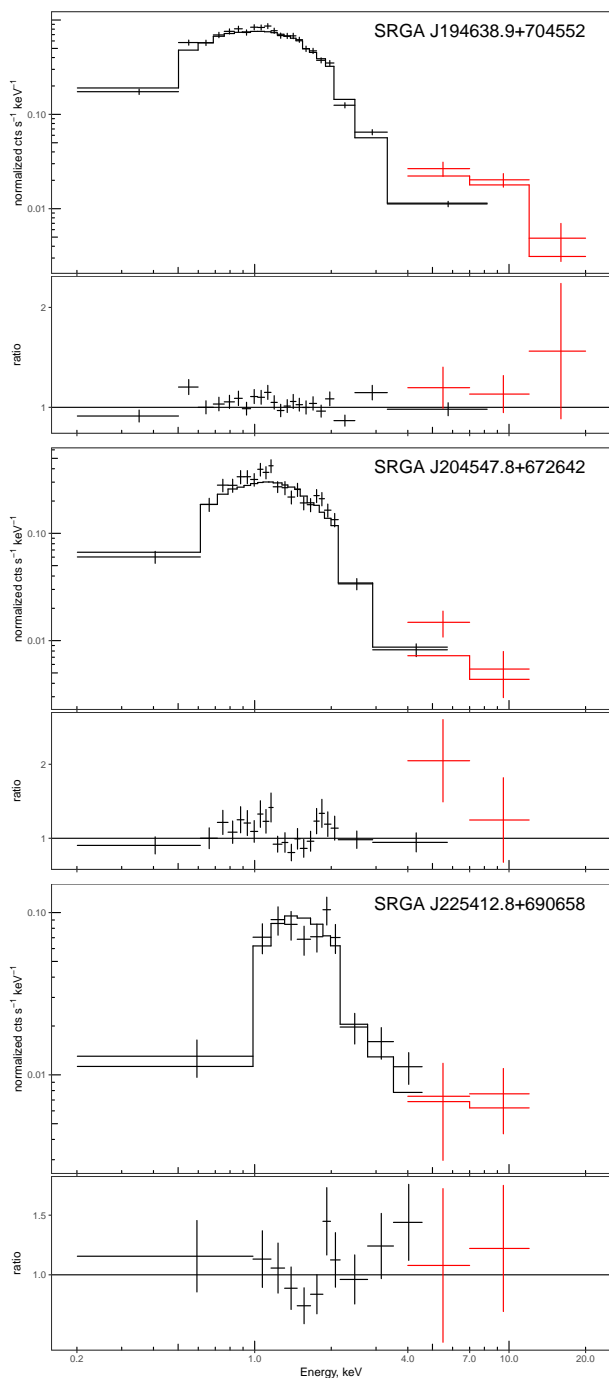


Fig. 1. X-ray spectra (upper panels) obtained by eROSITA (black) and ART-XC (red) and their best-fit $\text{PHABS}^*\text{BREMSS}$ models. The lower panels show the corresponding data-to-model ratio plots. The horizontal line indicates a ratio of 1.

4. Optical observations

For each of the three X-ray sources, the archival optical images show a single relatively bright star within the eROSITA location region (Fig. 2). These stars are known to be variable from previous observations, which corroborates that these are CVs.

Some key optical characteristics of these objects are listed in Table 4 and are discussed in Section 4.3 below. Specifically, for each star, we provide the parallax distance based on Gaia Collaboration et al. (2021), the apparent visual magnitude and the amplitude of its variability, the interstellar extinction to the object,

Table 4. Optical properties of the CVs.

| Object | D^a , pc | V | ΔV^b | A_V^c | M_V |
|-----------------------|---------------|-------|--------------|---------|-------|
| SRGA J194638.9+704552 | 1816 ± 43 | 14.16 | ± 0.23 | 0.5 | 2.3 |
| SRGA J204547.8+672642 | 848 ± 9 | 13.83 | ± 0.34 | 0.9 | 3.3 |
| SRGA J225412.8+690658 | 686 ± 12 | 16.46 | ± 2.11 | 2.4 | 4.9 |

Notes. ^(a) Distance based on Gaia Collaboration et al. (2021).

^(b) Variability amplitude based on ZTF and ASAS-SN data.

^(c) Extinction based on Schlegel et al. (1998); Schlafly & Finkbeiner (2011), and Green et al. (2019).

and the absolute visual magnitude. Our estimates of the extinction are based on (i) the Schlegel et al. (1998) dust map (SFD) recalibrated according to Schlafly & Finkbeiner (2011), which provides the total Galactic extinction in a given direction⁴, and (ii) the Bayestar19 model of the three-dimensional dust distribution in the Galaxy (Green et al. 2019), which allows the distance to the object to be taken into account⁵. We adopt $R_V = 3.1$ and $R_{g-r} = E(g-r)/E(B-V) = 0.98 \pm 0.02$ (Schlafly & Finkbeiner 2011) to convert $E(B-V)$ and $E(g-r)$ into visual extinction, A_V . The SFD and Bayestar19 estimates of A_V prove to not differ significantly from each other for the stars under consideration, which is expected because of their large distances and fairly high altitudes above the Galactic plane.

4.1. Spectroscopy

To study these objects in detail, we conducted follow-up optical observations with the Sayan Observatory 1.6 m AZT-331K telescope. For spectroscopy, we used the ADAM low- and medium-resolution spectrograph (Afanasiev et al. 2016; Burenin et al. 2016a). The observations were made using the VPHG600G volume-phase holographic grating, which provides the $3650\text{\AA} - 7250\text{\AA}$ spectral range and $\sim 9\text{\AA}$ spectral resolution with a $2''$ slit. The typical image quality was about $1''.8-2''$. During the observations of each object, halogen and He-Ne-Ar lamp calibration spectra were obtained after a series of spectroscopic images. After each exposure, we shifted the position of the object along the slit by $10''-15''$ in a random direction to reduce the interference fringes in the spectra. We processed the data using the IRAF⁶ software package and our own software. Spectral fluxes were calibrated using observations of spectrophotometric standards from the ESO list⁷.

To estimate the intrinsic width of emission lines, we quadratically subtracted the instrument line broadening from the line widths measured from the observed spectra. The correction of the spectra for extinction was made using the IRAF *deredden* task. The extinction for each object was estimated as described below.

4.2. Photometry

During the period from 17 to 20 June 2021, we conducted photometric observations of the objects using the CCD photometer of the AZT-331K telescope. It consists of a focal reducer and the Andor iKon-M 934 camera with the BD_DD 1024 \times 1024 detector, which provide a $6.3' \times 6.3'$ field of view with a $0''.372$ pixel

⁴ <https://irsa.ipac.caltech.edu/applications/DUST/>

⁵ <http://argonaut.skymaps.info/>

⁶ <http://iraf.noao.edu>

⁷ <https://www.eso.org/sci/observing/tools/standards/spectra.html>

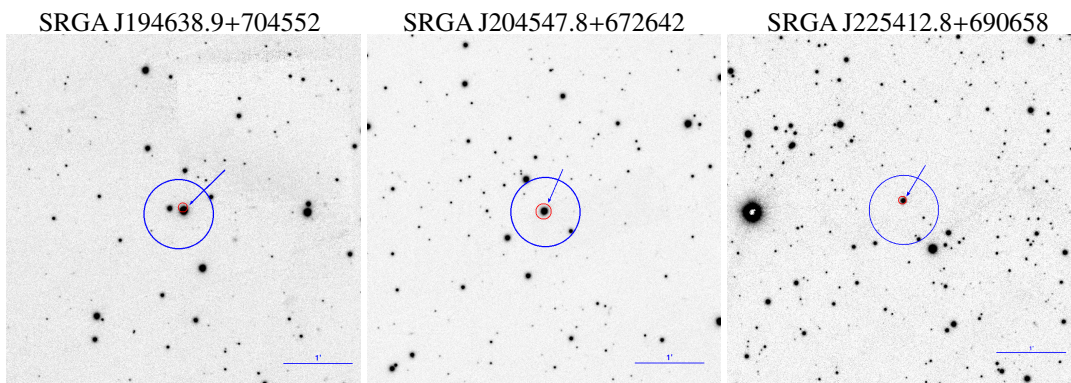


Fig. 2. Pan-STARRS1 images in the r filter around SRGA J194638.9+704552 (left), SRGA J204547.8+672642 (middle), and SRGA J225412.8+690658 (right). The size of each image is $5' \times 5'$. The blue circle with a radius of $30''$ indicates the ART-XC location. The red circle shows the eROSITA 98% location region. The optical counterpart is indicated by the arrow.

Table 5. Log of optical observations with the AZT-33IK telescope.

| Object | Date | Spectroscopy | | | Photometry | | |
|-----------------------|------------|------------------|----------|-------|------------|-------------------|--------|
| | | Exp. time | Grism | Slit | Date | Exp. time | Filter |
| SRGA J194638.9+704552 | 2020-10-23 | 3×60 s | VPHG600G | $2''$ | 2021-06-17 | 420×15 s | r |
| SRGA J204547.8+672642 | 2020-10-21 | 3×200 s | VPHG600G | $2''$ | 2021-06-18 | 540×15 s | r |
| SRGA J225412.8+690658 | 2021-05-14 | 5×100 s | VPHG600G | $2''$ | 2021-06-19 | 240×30 s | r |

Notes. The exp. time columns show the number of obtained images during continuous observations and the exposure time of each frame. The date columns show the observation dates in the YYYY-MM-DD format, UTC+0.

scale. For each object, the observations were carried out continuously for 2 hours or more. The quality of direct images was not worse than $1''.7$ in the SDSS r filter.

We processed the images in a standard way using `IRAF` and our own software. Aperture photometry was made using the `ap-phot` task from the `IRAF digiphot` package. The source fluxes were measured relative to nearby bright stars, with the aperture size for each observation series defined such that the maximum possible S/N was obtained.

We calibrated the measured magnitudes using the magnitudes of secondary photometric standards in the source field with a brightness comparable to or greater than the flux of the CV candidates. We used point-spread-function magnitudes from Pan-STARRS1 DR2 (Chambers et al. 2016) for calibration. The processing of light curve data was performed using the `Python Lightkurve` package (Lightkurve Collaboration et al. 2018). Further details of the optical observations are given in Table 5.

4.3. Results

Figure 3 shows the measured optical spectra and light curves. Table 6 presents the characteristics of the emission lines detected in the spectra. We now discuss the results of archival and follow-up optical observations on a source-by-source basis.

4.3.1. SRGA J194638.9+704552

This X-ray source is identified with the source ID 2263241129823231104 in the *Gaia* EDR3 catalog. According to the UCAC4 catalog (Zacharias et al. 2012), it has average magnitudes $B = 15.00$ and $V = 14.16$. The object has also been observed in the Zwicky Transient Facility (ZTF⁸) survey with the Palomar Observatory 48-inch Samuel Oschin Telescope.

⁸ <https://www.ztf.caltech.edu/>

The transient ZTF18absajkj⁹ was discovered on 31 August 2018, and was rediscovered as transient ZTF19acyzjtl on 25 November 2019. According to the Automatic Learning for the Rapid Classification of Events (ALeRCE¹⁰) (Sánchez-Sáez et al. 2021; Förster et al. 2021), it is more likely to be a CV than a cepheid or eclipsed binary star. Its mean magnitudes in the ZTF filters (Bellm et al. 2019) are $g_{mean} = 14.54$ and $r_{mean} = 13.74$. Based on the ZTF light curve, which spans ~ 3 years, we can estimate the amplitude of the source variability at $\Delta V = \pm 0.23$.

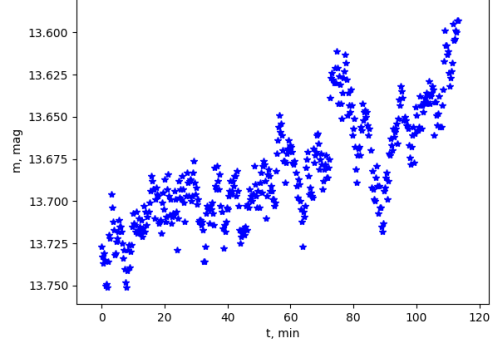
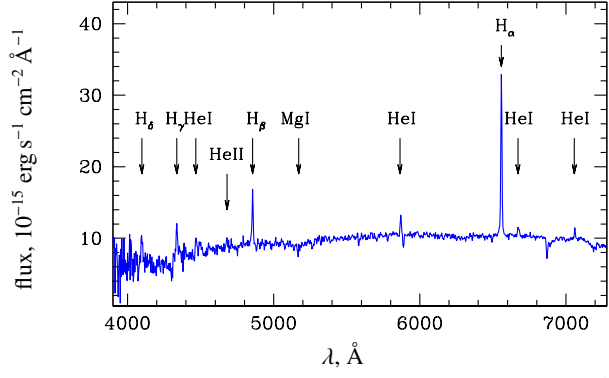
The spectrum of the object (see Fig. 3) is typical of CVs (e.g., Warner 1995). Specifically, it shows a series of hydrogen and helium emission lines. Some Fraunhofer absorption lines are also visible. The Balmer decrement $H_\alpha/H_\beta = 3.4 \pm 0.4$ (hereafter, the quoted uncertainties are at 1σ confidence level, unless noted otherwise), which indicates a moderate extinction if an intrinsic ratio $H_\alpha/H_\beta = 2.86$ is adopted (Osterbrock 1989). Using the $E(B - V) = 1.97 \log_{10}[(H_\alpha/H_\beta)_{obs}/2.86]$ relation from Osterbrock (1989), we obtain $E(B - V) = 0.15 \pm 0.10$, which is consistent with the interstellar extinction to the source.

During the 114 minutes of AZT-33IK photometry, we obtained 15 images with an exposure of 420 s. Over this period, the reference star magnitude varied by 0.008^m (root-mean square), while SRGA J194638.9+704552 exhibited much stronger variations (see Fig. 3). Because the intervals between the individual exposures were not strictly constant, we used a Lomb–Scargle periodogram (Lomb 1976; Scargle 1982) for the timing analysis. The derived power spectrum (not shown) reveals strong red-noise-like variability (already obvious from the high-amplitude stochastic fluctuations in the light curve) modified by a window function. There are no signs of periodicity or quasi-periodicity. Due to the window function, it is difficult to place upper limits on the amplitude of any periodic signal. However, the general

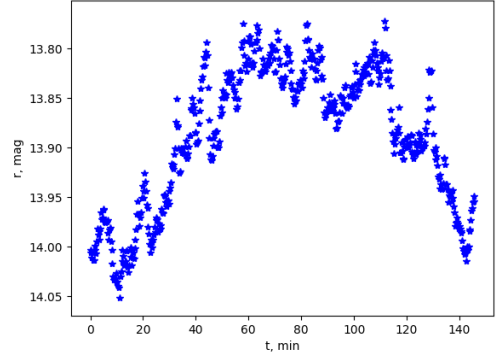
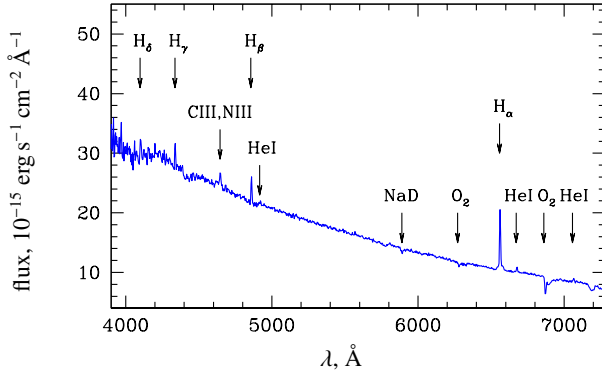
⁹ <https://alerce.online/object/ZTF18absajkj>

¹⁰ <http://alerce.science/>

SRGA J194638.9+704552



SRGA J204547.8+672642



SRGA J225412.8+690658

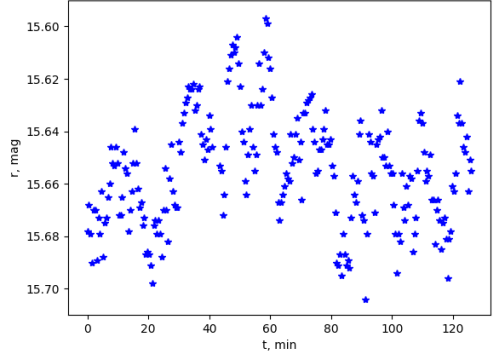
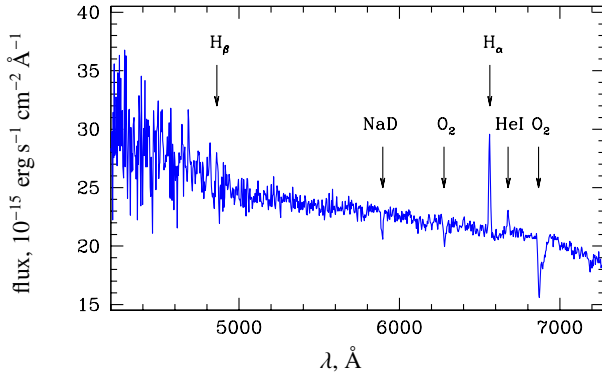


Fig. 3. Optical spectra (left) and light curves (right) of the objects. The spectra are corrected for interstellar extinction, and prominent spectral features are indicated. The light curves are obtained in the SDSS r filter, and the time is measured from the beginning of the observation.

rising trend evident in the light curve suggests that the orbital period of this CV is longer than 2 hours.

If this object were a magnetic CV, we might expect to see signs of the white dwarf spin period in its light curve, which are usually in the range of ~ 1 min to ~ 1 hour for this class of objects (e.g., Mukai 2017). However, spin modulation is not always evident in the optical light of magnetic CVs, thus its absence in the optical light curve of SRGA J194638.9+704552 does not rule out a polar or intermediate polar origin.

4.3.2. SRGA J204547.8+672642

This X-ray source is identified with the nonperiodic variable star ASASSN-V J204548.04+672643.0¹¹ from the All Sky Automated Survey for SuperNovae (ASAS-SN) catalog of variable stars VI (Jayasinghe et al. 2020), with an average V magnitude $V_{mean} = 13.83$ and an amplitude of variations $\Delta V = 0.34$. In the *Gaia* EDR3 catalog, the object is listed as source ID 2246133514871244672.

The object has also been observed by the *Transiting Exoplanet Survey Satellite* (TESS, Ricker et al. 2014) in sectors 15,

¹¹ <https://asas-sn.osu.edu/variables/AP15943107>

SRGA J204547.8+672642

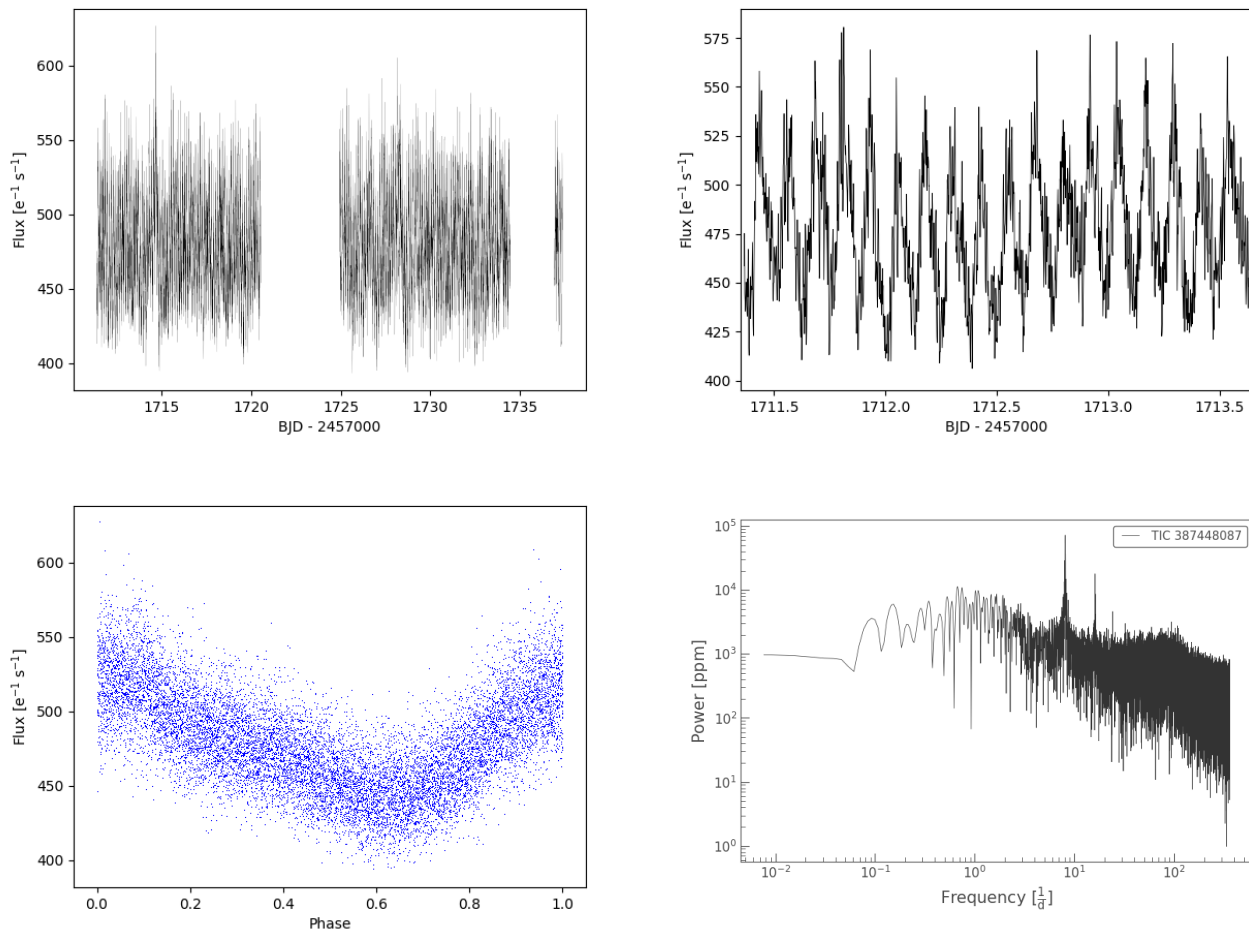


Fig. 4. *TESS* observations of SRGA J204547.8+672642. Top row: light curves obtained in sector 15 (full data set on the left, and the first two days of observations on the right). Bottom left: Light curve folded on the 2.98-hour period. Bottom right: Lomb–Scargle periodogram.

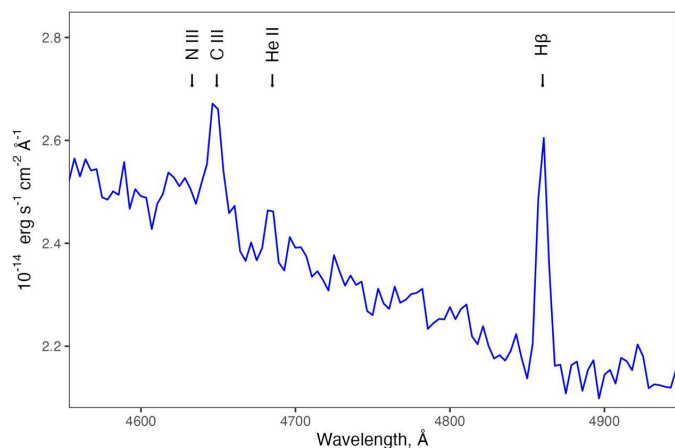


Fig. 5. Zoom into the 4550–4950 \AA range of the optical spectrum of SRGA J204547.8+672642. The Bowen blend and H β are visible, while HeII λ 4686 is not significantly detected.

16, 17, 18, 24, and 25, with 2- and 30-minute cadences. We performed a timing analysis of the data obtained in sector 15 with a 2-minute cadence. Figure 4 shows the resulting light curve and a Lomb–Scargle periodogram that is based on it. The periodogram

reveals a 2.979 ± 0.006 -hour periodic signal (and its harmonics) as well as a strong and complex variability. The derived period is typical of the orbital periods of CVs (e.g., Warner 1995). In the variability power spectrum, we can also distinguish a break of the continuum at $\sim 10^{-3}$ Hz, which is also typical of CVs (Revnivtsev et al. 2010; Scaringì et al. 2015).

The optical spectrum (Fig. 3) of the object reveals emission lines of the Balmer series from H α to H δ as well as emission lines of helium: HeI λ 4922, HeI λ 6678, and HeI λ 7065. The CIII + NIII λ 4640, 4650 Bowen blend is also visible (see Fig. 5), but the HeII λ 4686 and HeI λ 5876 lines are not significantly detected. Overall, these spectral features are characteristic of CVs, especially of polars (Warner 1995). The Balmer decrement $H\alpha/H\beta = 3.5 \pm 0.9$. This corresponds to a reddening of $E(B - V) = 0.17 \pm 0.22$, which is consistent with the interstellar extinction to the source.

During the 146 minutes of AZT-33IK photometry, we obtained 540 images with an exposure of 15 s. Over this period, the reference star magnitude varied by 0.005^m (rms), while SRGA J204547.8+672642 exhibited much stronger variations (see Fig. 3). The behavior of this short-term light curve is consistent with the 2.98-hour orbital modulation unveiled in the *TESS* long-term light curve.

Table 6. Optical emission lines.

| Lines | Wavelength ^a Å | Flux ^b 10 ⁻¹⁴ erg s ⁻¹ cm ⁻² | Eq. width ^c Å | FWHM km s ⁻¹ |
|-----------------------|------------------------------|---|--------------------------------------|----------------------------|
| SRGA J194638.9+704552 | | | | |
| H _δ | 4098.2 | < 2.6 | – | – |
| H _γ | 4337.2 | 2.5 ^{+1.4} _{-0.5} | -6.0 ^{+5.5} _{-1.4} | 337 ± 57 |
| HeIλ4471 | 4468 | < 2.9 | – | – |
| HeIIλ4686 | 4680 | < 2.1 | – | – |
| H _β | 4856.7 | 4.3 ± 0.5 | -8.2 ± 0.6 | 238 ± 48 |
| HeIλ5876 | 5870.4 | 2.1 ^{+0.7} _{-0.4} | -3.2 ^{+0.9} _{-0.6} | 336 ± 73 |
| H _α | 6558.6 | 14.8 ± 0.8 | -20.8 ± 2.1 | 205 ± 36 |
| HeIλ6678 | 6675.1 | < 1.5 | – | – |
| HeIλ7065 | 7060.1 | < 1.1 | – | – |
| SRGA J204547.8+672642 | | | | |
| H _δ | 4101.9 | < 1.6 | – | – |
| H _γ | 4338.2 | 1.1 ^{+0.5} _{-0.2} | -1.2 ^{+0.5} _{-0.2} | 240 ± 90 |
| CIII, NIII | | | | |
| λλ4640, 4650 | 4647.4 | 1.2 ^{+0.8} _{-0.3} | – | – |
| HeIIλ4686 | 4684 | < 0.5 | – | – |
| H _β | 4860.0 | 1.4 ± 0.4 | -1.7 ± 0.5 | 156 ± 64 |
| HeIλ4922 | 4922.3 | < 0.6 | – | – |
| H _α | 6562.1 | 4.9 ± 0.3 | -9.2 ± 0.9 | 100 ± 23 |
| HeIλ6678 | 6678.5 | < 0.6 | – | – |
| HeIλ7065 | 7065.5 | < 0.6 | – | – |
| SRGA J225412.8+690658 | | | | |
| H _β | 4862.6 | < 7.9 | – | – |
| H _α | 6561.5 | 16.9 ± 2.0 | -5.0 ± 0.7 | 188 ± 42 |
| HeIλ6678 | 6677.1 | 4.3 ± 1.1 | -1.2 ± 0.3 | 222 ± 141 |

Notes. (a) Measured line wavelength.

(b) The fluxes are not corrected for the interstellar extinction. Upper limits are provided for lines with an S/N lower than 2σ.

(c) Negative values correspond to emission lines. Uncertainties correspond to the 1σ (68%) confidence interval.

4.3.3. SRGA J225412.8+690658

This X-ray source is identified with a nonperiodic strongly variable star¹² from the ASAS-SN catalog of variable stars I (Jayasinghe et al. 2018), with $V_{mean} = 16.46$ and $\Delta V = 2.11$. In this catalog, the object is classified as a young stellar object with a classification probability of 0.528. In the *Gaia* EDR3 catalog, the object is listed as source ID 2225473558247025152.

The optical spectrum of the object (Fig. 3) shows H_α and HeIλ6678 emission lines, a weak H_β emission line, and absorption lines of Na (λ5890) and O₂. Only a lower limit can be placed on the Balmer decrement: H_α/H_β > 2.1. The absence of emission lines in the short-wave part of the spectrum is likely due to the much higher extinction toward SRGA J225412.8+690658 compared to SRGA J194638.9+704552 and SRGA J204547.8+672642.

During the 127 minutes of AZT-33IK photometry, we obtained 240 images with an exposure of 30 s. The last 30 minutes of observations were made at dusk, at a Sun altitude of (-12°, -16°) degrees. As a result, the magnitudes measured after 90 minutes from the start have a lower S/N. The light curve of the object (see Fig. 3) exhibits modest variations, which are, however, much greater than the deviations in the light curve of the reference star (0.011^m rms). It is impossible to draw any conclusions on an orbital or other periodicity based on this short-term light curve.

Based on the absolute magnitude $M_V \sim 4.8$, the luminosity of the object is too low for Be stars, which are also characterized

¹² <https://asas-sn.osu.edu/variables/468427>

by emission lines of the Balmer series. Furthermore, the variability of the object is too high for Be stars, $\Delta V = \pm 2.1$. Together with the X-ray luminosity and spectrum, this strongly indicates that SRGA J225412.8+690658 is a CV.

5. Discussion

We can use the measured X-ray fluxes, *Gaia* distances, and absolute optical magnitudes to estimate the X-ray and optical luminosities of the objects. This information and that on the equivalent width (*EW*) of the H_β line in the optical spectra is given in Table 7. For SRGA J225412.8+690658, only an upper limit on *EW* (H_β) is available.

The measured X-ray luminosities are typical of CVs (e.g., Sazonov et al. 2006; Mukai 2017). The fairly high L_X/L_V ratios ($\sim 0.1 - 0.5$) found for the objects indicate moderate accretion rates ($\dot{M} \sim$ a few $\times 10^{15}$ – a few $\times 10^{17}$ g s⁻¹) onto the white dwarf (Patterson & Raymond 1985)¹³. This appears to be consistent with their fairly high X-ray luminosities, taking into account the large intrinsic scatter in the L_X/L_V versus \dot{M} and L_X versus \dot{M} relations for CVs (see figs. 6 and 7 in Patterson & Raymond 1985) and the substantial optical variability of the objects studied here. The obtained values of L_X/L_V and *EW* (H_β) similarly agree satisfactorily with the known correlation of these quantities for CVs (Patterson & Raymond 1985).

With $L_X \sim 3 \times 10^{33}$ erg s⁻¹ (2–10 keV), it is highly likely that SRGA J194638.9+704552 is an intermediate polar. SRGA J204547.8+672642 and SRGA J225412.8+690658, both having $L_X \sim 2 \times 10^{32}$ erg s⁻¹, are also likely to be magnetic CVs, but their luminosities can also pertain to nonmagnetic CVs (dwarf novae). The optical spectrum of SRGA J204547.8+672642 includes a CIII + NIIIλ4640, 4650 Bowen blend, the flux in which is comparable to the flux in H_β. This suggests that the object may be a polar (Schachter et al. 1991; Warner 1995), although this spectral feature can also be observed in intermediate polars (e.g., Harlaftis & Horne 1999). Furthermore, the bright absolute magnitude, $M_V = 3.3$, and the moderate optical variability, $\Delta V = \pm 0.3$, are not typical of dwarf novae (Warner 1995). The same is true for SRGA J194638.9+704552, for which $M_V = 2.3$ and $\Delta V = \pm 0.2$.

6. Conclusion

We reported the discovery of three CV candidates in the 4–12 keV ART-XC source catalog obtained after the first year of the *SRG* all-sky survey (Pavlinisky et al. 2021a). These sources have also been detected by the eROSITA telescope on board the *SRG*. All three objects were previously known as X-ray sources from the *ROSAT* all-sky survey and *XMM-Newton* slew survey, but their nature has remained unknown.

The X-ray spectra obtained by eROSITA and ART-XC in the 0.2–20 keV energy range for SRGA J194638.9+704552 and in the 0.2–12 keV band for SRGA J204547.8+672642 and SRGA J225412.8+690658 are consistent with optically thin thermal emission with a temperature $kT \gtrsim 18$ keV for SRGA J194638.9+704552 and SRGA J225412.8+690658 and $kT \gtrsim 5$ keV for SRGA J204547.8+672642. Together with the inferred high X-ray luminosities ($2 \times 10^{32} - 3 \times 10^{33}$ erg s⁻¹), this strongly suggests that all three sources are CVs.

¹³ These authors used the 0.2–4 keV energy band, while we use 2–10 keV; however, the ratio of the fluxes in these bands is close to unity, $F(2 - 10)/F(0.2 - 4) \sim 1 - 1.5$, for optically thin emission with $kT \gtrsim 5$ keV, as is the case for the objects under consideration.

Table 7. Physical properties of the CVs

| Object | L_V , erg s ⁻¹ | L_X , erg s ⁻¹ | $\log(L_X/L_V)$ | $EW(H\beta)$, Å |
|-----------------------|------------------------------------|--------------------------------|------------------|------------------|
| SRGA J194638.9+704552 | $(4.8 \pm 0.9) \times 10^{33}$ | $(2.7 \pm 0.2) \times 10^{33}$ | -0.26 ± 0.09 | 8.2 ± 0.6 |
| SRGA J204547.8+672642 | $(1.9 \pm 0.5) \times 10^{33}$ | $(2.6 \pm 0.2) \times 10^{32}$ | -0.87 ± 0.12 | 1.7 ± 0.5 |
| SRGA J225412.8+690658 | $0.5^{+2.9}_{-0.4} \times 10^{33}$ | $(1.6 \pm 0.2) \times 10^{32}$ | -0.49 ± 0.84 | < 3.2 |

Notes. L_X is the X-ray luminosity in the 2–10 keV energy band, based on the eROSITA and ART-XC data and the best-fit power-law spectral models from Table 3, corrected for the Galactic absorption.

We have conducted optical photometry and spectroscopy of these objects using the AZT-33IK 1.6 m telescope of the Sayan Observatory. The optical properties confirm the CV nature of the objects. We conclude that SRGA J194638.9+704552 is an intermediate polar, SRGA J204547.8+672642 likely is a polar or intermediate polar, and SRGA J225412.8+690658 may be a magnetic or nonmagnetic CV. We also measured an orbital period of 2.98 hours for SRGA J204547.8+672642 based on archival *TESS* data.

This research is a continuation of the work of optically identifying X-ray sources (Zaznobin et al. 2021) that were detected during the ART-XC all-sky survey. Three out of the planned eight *SRG* all-sky surveys have now been completed. We expect to find many new CVs during this survey and will continue our optical follow-up program.

Acknowledgements. We appreciate helpful suggestions from the referee. The measurements with the AZT-33IK telescope were performed within the basic financing of the FNI II.16 program and were obtained using the equipment of the Angara sharing center¹⁴. In this study, we used observational data from the eROSITA and ART-XC telescopes on board *SRG*. The *SRG* observatory was built by Roskosmos in the interests of the Russian Academy of Sciences represented by its Space Research Institute (IKI) within the framework of the Russian Federal Space Program, with the participation of the Deutsches Zentrum für Luft- und Raumfahrt (DLR). The *SRG*/eROSITA X-ray telescope was built by a consortium of German Institutes led by MPE, and supported by DLR. The *SRG* spacecraft was designed, built, launched, and is operated by the Lavochkin Association and its subcontractors. The science data are downlinked via the Deep Space Network Antennae in Bear Lakes, Ussurijsk, and Baykonur, funded by Roskosmos. The eROSITA data used in this work were processed using the *eSASS* software system developed by the German eROSITA consortium and the proprietary data reduction and analysis software developed by the Russian eROSITA Consortium. This work was supported by grant no. 21-12-00210 from the Russian Science Foundation.

References

Afanasyev, V. L., Dodonov, S. N., Amirkhanyan, V. R., & Moiseev, A. V. 2016, *Astrophysical Bulletin*, 71, 479

Arnaud, K. A. 1996, in *Astronomical Society of the Pacific Conference Series*, Vol. 101, *Astronomical Data Analysis Software and Systems V*, ed. G. H. Jacoby & J. Barnes, 17

Bellm, E. C., Kulkarni, S. R., Graham, M. J., et al. 2019, *PASP*, 131, 018002

Boller, T., Freyberg, M. J., Trümper, J., et al. 2016, *A&A*, 588, A103

Burenin, R. A., Amvrosov, A. L., Eselevich, M. V., et al. 2016a, *Astronomy Letters*, 42, 295

Burenin, R. A., Revnitvsev, M. G., Tkachenko, A. Y., et al. 2016b, *Astronomy Letters*, 42, 240

Byckling, K., Mukai, K., Thorstensen, J. R., & Osborne, J. P. 2010, *MNRAS*, 408, 2298

Chambers, K. C., Magnier, E. A., Metcalfe, N., et al. 2016, arXiv e-prints, arXiv:1612.05560

Förster, F., Cabrera-Vives, G., Castillo-Navarrete, E., et al. 2021, *AJ*, 161, 242

Gaia Collaboration, Brown, A. G. A., Vallenari, A., et al. 2021, *A&A*, 649, A1

Goodman, J. & Weare, J. 2010, *Communications in Applied Mathematics and Computational Science*, 5, 65

Green, G. M., Schlafly, E., Zucker, C., Speagle, J. S., & Finkbeiner, D. 2019, *ApJ*, 887, 93

Harlaftis, E. T. & Horne, K. 1999, *MNRAS*, 305, 437

HI4PI Collaboration, Ben Bekhti, N., Flöer, L., et al. 2016, *A&A*, 594, A116

Jayasinghe, T., Kochanek, C. S., Stanek, K. Z., et al. 2018, *MNRAS*, 477, 3145

Jayasinghe, T., Stanek, K. Z., Kochanek, C. S., et al. 2020, *MNRAS*, 493, 4186

Lightkurve Collaboration, Cardoso, J. V. d. M., Hedges, C., et al. 2018, *Lightkurve: Kepler and TESS time series analysis in Python*

Lomb, N. R. 1976, *Ap&SS*, 39, 447

Lutovinov, A., Suleimanov, V., Manuel Luna, G. J., et al. 2020, *New A Rev.*, 91, 101547

Mukai, K. 2017, *PASP*, 129, 062001

Oh, K., Koss, M., Markwardt, C. B., et al. 2018, *ApJS*, 235, 4

Osterbrock, D. E. 1989, *Astrophysics of gaseous nebulae and active galactic nuclei*

Patterson, J. & Raymond, J. C. 1985, *ApJ*, 292, 535

Pavlinisky, M., Sazonov, S., Burenin, R., et al. 2021a, *A&A* (in press)

Pavlinisky, M., Tkachenko, A., Levin, V., et al. 2021b, *A&A*, 650, A42

Predehl, P., Andritschke, R., Arefiev, V., et al. 2021, *A&A*, 647, A1

Pretorius, M. L. & Knigge, C. 2012, *MNRAS*, 419, 1442

Pretorius, M. L., Knigge, C., & Schwope, A. D. 2013, *MNRAS*, 432, 570

Revnitvsev, M., Burenin, R., Bikmaev, I., et al. 2010, *A&A*, 513, A63

Revnitvsev, M., Sazonov, S., Krivonos, R., Ritter, H., & Sunyaev, R. 2008, *A&A*, 489, 1121

Ricker, G. R., Winn, J. N., Vanderspek, R., et al. 2014, in *Society of Photo-Optical Instrumentation Engineers (SPIE) Conference Series*, Vol. 9143, *Space Telescopes and Instrumentation 2014: Optical, Infrared, and Millimeter Wave*, ed. J. Oschmann, Jacobus M., M. Clampin, G. G. Fazio, & H. A. MacEwen, 914320

Sánchez-Sáez, P., Reyes, I., Valenzuela, C., et al. 2021, *AJ*, 161, 141

Saxton, R. D., Read, A. M., Esquej, P., et al. 2008, *A&A*, 480, 611

Sazonov, S., Revnitvsev, M., Gilfanov, M., Churazov, E., & Sunyaev, R. 2006, *A&A*, 450, 117

Scargle, J. D. 1982, *ApJ*, 263, 835

Scaringi, S., Maccarone, T. J., Kording, E., et al. 2015, *Science Advances*, 1, e1500686

Schachter, J., Filippenko, A. V., Kahn, S. M., & Paerels, F. B. S. 1991, *ApJ*, 373, 633

Schlafly, E. F. & Finkbeiner, D. P. 2011, *ApJ*, 737, 103

Schlegel, D. J., Finkbeiner, D. P., & Davis, M. 1998, *ApJ*, 500, 525

Schwope, A. D., Brunner, H., Buckley, D., et al. 2002, *A&A*, 396, 895

Sunyaev, R., Arefiev, V., Babyshkin, V., et al. 2021, *A&A* (in press)

Warner, B. 1995, *Cataclysmic variable stars*, Vol. 28

Zacharias, N., Finch, C. T., Girard, T. M., et al. 2012, *VizieR Online Data Catalog*, I/322A

Zaznobin, I. A., Uskov, G. S., Sazonov, S. Y., et al. 2021, *Astronomy Letters*, 47, 71

¹⁴ <http://ckp-rf.ru/ckp/3056/>